UGVA-DPNC 1995/6-165 June 1995

Fermilab Library
0 1160 0048192 3

AN EXPERIMENTALIST'S HIGHLIGHTS †

J.H.FIELD
Département de Physique Nucléaire et Corpusculaire, Université de Genève
24, quai Ernest-Ansermet CH-1211Genève 4.
E-mail: jfield@cernvm.cern.ch

FERMILAB
AUG 1 1995
LIBRARY

ABSTRACT

A very limited selection is made among the wide range of new results presented at this workshop. Preference is given to topics where a fruitful confrontation between theory and experiment is possible. These include jet production studies, azimuthal correlation measurements, transition form factors of the light pseudoscalar mesons, and the reaction $\gamma\gamma \to \Lambda\bar{\Lambda}X$.

UGVA-DPNC-1995-6-165

1. Introduction

At this workshop, a total of 71 20 minute talks were given. Of these, 37 were experimental (15 $\gamma\gamma$, 18 γp and 4 on related fields), 26 were theoretical or phenomenological and 8 were on future projects. It is of course not possible to review all of this material in a meaningful way in a single 35 minute talk. I have rather chosen a limited number of topics where new experimental results have been shown that have a potentially important impact on our understanding of the physics of $\gamma\gamma$ or γp collisions. The choice made is necessarily a limited and personal one.

2. Photon Structure and Jet Production in γp and $\gamma\gamma$ Collisions

Results on the properties of 'remnant jets' [a]have been presented here for the first time for both γp [2,3,4] and $\gamma\gamma$[5] collisions. Photons may couple to a hadronic interaction where high p_T jets are produced in two distinct ways: (i) a 'direct' coupling, as in Fig.1a where the photon participates directly in the hard scattering process or (ii) a 'resolved' coupling where it is rather a partonic constituent (quark or gluon) that undergoes the hard scattering (Fig. 1b). In the second case the spectator constituents of the photon that do not interact continue to move within a limited angle[b] to the direction of the incident virtual photon, and form the 'remnant jet'.

In the case of a $2 \to 2$ hard scattering process, neglecting the p_T of the photon constituents, and assuming massless kinematics, the energy fractions x_γ, x_p of the interacting partons from the γ, p respectively, as shown for example in Fig.1, are

[a]Previously often refered to as 'beam-pipe jets' [1]

[b]This angle is expected to be smaller in the case of a VDM coupling of the photon where the constituent is that of a virtual vector meson, than for a point like coupling. In the latter case the distinction between 'resolved' and 'direct' components only makes sense if the p_T of the spectator quark is significantly less than that of the hard scattering process giving the high p_T jets

†*Invited talk at PHOTON'95 Sheffield 8 – 13 April 1995*

C15/04/08

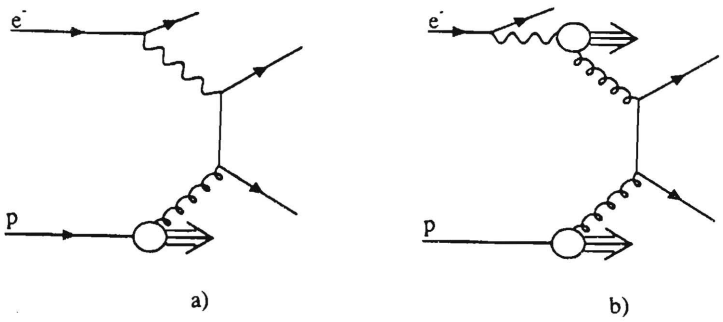

Figure 1: Examples of leading order diagrams for a) direct, b) resolved photoproduction

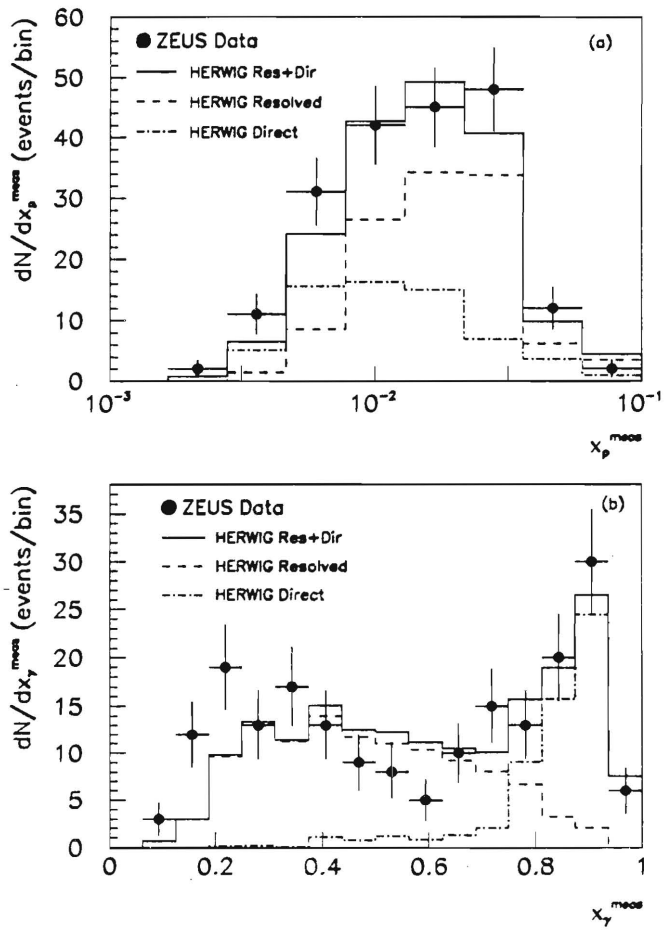

Figure 2: a) uncorrected x_p distribution, b) uncorrected x_γ distribution, for events with two or more jets (Ref.[3]).

given by:

$$x_\gamma = p_T \frac{[\exp(-\eta_1) + \exp(-\eta_2)]}{2E_\gamma} \tag{1}$$

$$x_p = p_T \frac{[\exp(\eta_1) + \exp(\eta_2)]}{2E_p} \tag{2}$$

η_1 and η_2 are the pseudorapidities of the high p_T jets :

$$\eta \equiv -\ln(\tan(\frac{\theta}{2})$$

$\theta = 0$ is along the incoming p direction and p_T is their common transverse momentum. The HERA detectors H1 and ZEUS are each equipped with a $\simeq 0°$ tagging system for the scattered electron. Magnetic spectrometers are used to measure the scattered electron energy E'_e and so determine the energy of the virtual photon from the relation $E_\gamma = E_e^{beam} - E'_e$. The measured jet angles and p_T then enable x_γ to be calculated using Eq.1. The ZEUS results for x_p, x_γ are shown in Fig.2a,b [3] in comparison with the predictions of the HERWIG [7] Monte Carlo generator. Clear evidence is seen in Fig.2b of both direct ($x_\gamma \simeq 1$) and resolved ($x_\gamma < 1$) contributions. For small values of x_γ the cross-section is dominated by the effect of the gluon density $g(x_\gamma)$ of the photon, as shown in Fig.1b. The H1 result [4] for $x_\gamma g(x_\gamma)$ is shown in Fig.3. The dramatic rise at small x_γ of $g(x_\gamma)$ predicted by the LAC1[8] gluon density is not confirmed. On the other hand the GRV-LO [9] prediction agrees well with the measurement.

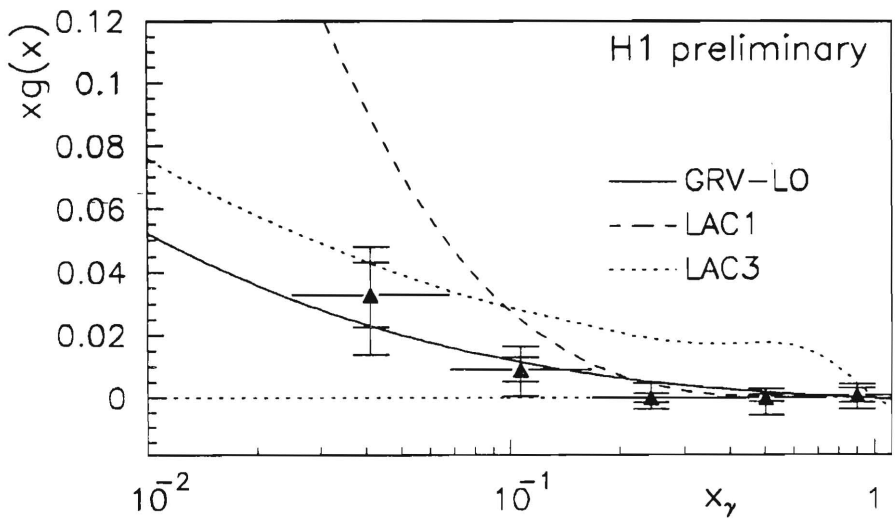

Figure 3: LO estimate of the gluon density of the photon unfolded using PYTHIA from events with two jets having $E_t^{jet} > 7GeV$ and $\eta^{jet} < 2.5$ (Ref[4]).

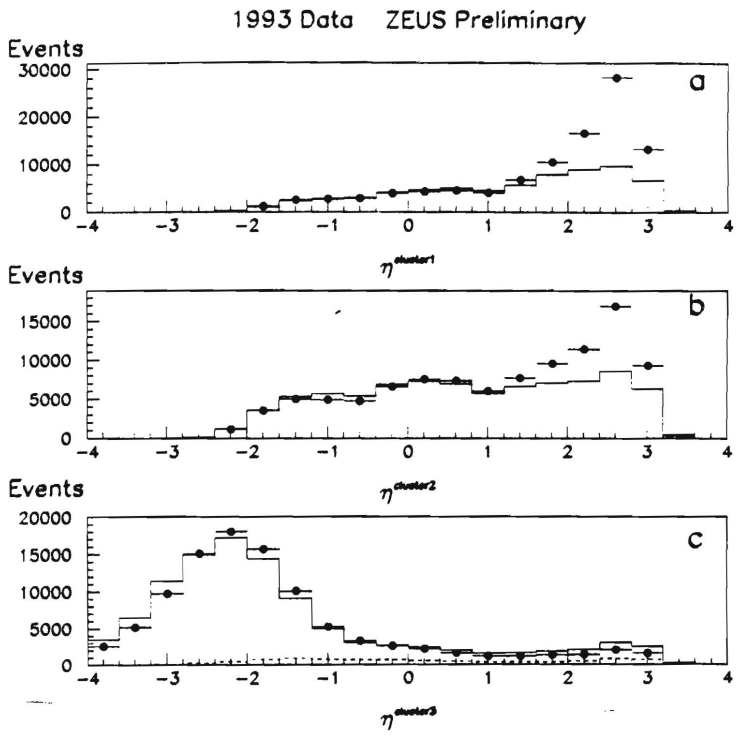

Figure 4: Pseudorapidity (η) distributions of the first a), second b) and third c) clusters found by the k_T alogorithm: ZEUS data (full cicles), MC direct+resolved (full histogram) and MC direct (dashed histogram). Data and MC events are normalised in the region $\eta \leq 1.6$ (Ref.[2]).

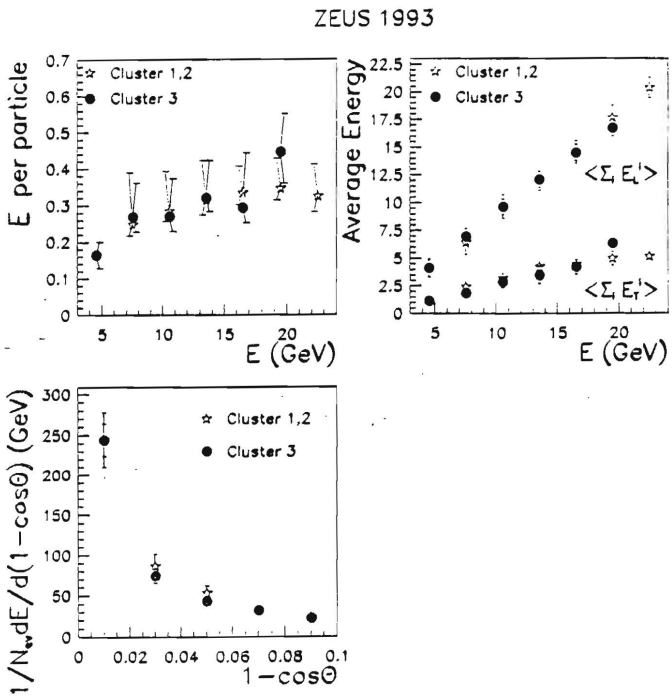

Figure 5: Comparison of the internal kinematical properties of the remnant jet (Cluster 3) with those of the two higher p_T jets (Clusters 1,2). E_L, E_T, θ of the particles in the jet are defined relative to the jet axis (Ref.[2]).

More details on the properties of the Remnant Jets in low Q^2 ep collisions were presented by Behrens (ZEUS Collaboration)[2]. A sample of events with transverse energy $> 15GeV$ was classified into exactly three jets using a k_T clustering algorithm[10,11]. The jets were then ordered in p_T with :

$$p_T^{jet1} > p_T^{jet2} > p_T^{jet2}$$

The corresponding pseudorapidity distributions are shown in Fig. 4a,b,c. The prediction of the PYTHIA Monte Carlo[12] (normalised for $\eta^{jet} < 1.6$) is also shown. 92 % of the events are predicted to be resolved, 8 % direct. The photon remnant jet is visible as the large enhancement for negative η in Fig.4c. In Fig.5 some internal kinematical quantities of the remnant jet (cluster3) are compared with those of the two highest p_T jets (clusters1,2). The jets are seen to be identical within the experimental errors. The same quantities of all three jets are well described by PYTHIA.

Evidence for doubly resolved events in untagged $\gamma\gamma$ collisions was presented by Hayashi [5]. The wide acoplanarity distribution observed between the two high p_T jets in the resolved events may be evidence for a contribution of point-like photon-quark couplings in these events.

In an interesting analysis of charm pair production in $\gamma\gamma$ collisions [6] the presence of a single remnant jet was used to tag the resolved production of such pairs (i.e. via the process $\gamma g \rightarrow c\bar{c}$ where the gluon g is a photon constituent, rather than via the direct process $\gamma\gamma \rightarrow c\bar{c}$).Separate cross-sections were presented for 'resolved' and 'direct' charm pair production. A low value of the charm quark mass of 1.3 GeV and the LAC1 gluon density function (which, as shown above, is not compatible with the H1 measurement of $g(x_\gamma)$) was found necessary to describe the data. For more discussion of $\gamma\gamma \rightarrow c\bar{c}$ cross-sections see Ref.13.

Measurements of remnant jet properties such as those reported in Refs.[2-6] can lead to a deeper and more quantitative understanding of the difference between the 'hadronic' and 'point-like' parts of the photon structure function. The importance of the final state event structure in making such a separation was pointed out many years ago[14,15]. The remnant jet data presented at this workshop has come largely from photoproduction by quasi-real virtual photons or untagged $\gamma\gamma$ events, and so is largely dominated by the hadronic (VDM) part of the photon parton densities[c] It may be remarked that direct measurement of the energy E_{REM} of the remnant jet gives an alternative way to determine x_γ, i.e.

$$x_\gamma = (E_\gamma - E_{REM})/E_\gamma \tag{3}$$

[c]It is common in the literature to use the same expression 'structure function' both for a true structure function which is a total cross-section for initial state photons of well defined helicity, and for a parton density that describes the probability that a photon branches into a virtual parton of given energy and p_T, both complimentary to those of the associated remnant jet. A parton density is a distribution that is defined only as a factor inside an integral. This essential difference is often neglected in phenomenological applications, leading to double counting [16].

In the case of a point-like contribution to the resolved cross-section (also reflected in the higher p_T for the remnant jet) a harder x_γ distribution is to be expected, than in the case of the hadronic (VDM) contribution. The characteristic exponential p_T fall-off associated with the VDM photon quark coupling was already clearly seen in PETRA data on $\gamma\gamma$ collisions [17,18]. The crucial rôle of this 'spectator p_T' (or equivalently the virtuality t of the off-shell quark coupling to the photon target) in determining the 'hadronic' or 'point-like' behaviour of the photon structure function was first shown by Llewellyn-Smith[19]. In fact it is the minimum kinematically allowed value of this virtuality, t_{MIN} that contains *all the relevant scales* P^2 (target mass), m_q^2 (quark mass), $(p_T^{MIN})^2$ (VDM, point- like separation), necessary to define the point-like photon structure function at lowest order in QCD:

$$t_{MIN}(x) = \frac{m_q^2 + p_T^{MIN}(x)^2}{1-x} + xP^2 \tag{4}$$

It is important to note that t_{MIN} is not a constant, but a function of x. A procedure to phenomenologicaly determine the function $p_T^{MIN}(x)$ was given in Ref.20. Although the importance of the p_T of the remnant quark in the definition of the'hadronic' and 'point-like' pieces of the photon structure function has been fully taken into account in recent Monte Carlo generators [21], this is not however the case, (as also pointed out in Ref.[22]), in more recent, and closely related, theoretical work [23].

3. Azimuthal Correlations in Photon Photon Interactions

New work both theoretical [24] and experimental [25] on azimuthal correlations was presented at the workshop. In the case that a two body final state is produced and both scattered electrons are observed, two independant azimuthal angles ϕ, ϕ_a may be defined. In the $\gamma\gamma$ C.M. frame ϕ is the angle between the planes defined by the incoming and scattered e^+, e^- while ϕ_a is that between the planes defined by the incoming and scattered e^+ and that spanning the $\gamma\gamma$ axis and direction of one of the outgoing particles (say the μ^+ in the case of the $\mu^+\mu^-$ final state). For multiple particle final states ϕ_a may be defined using any outgoing particle, leading to a one particle inclusive azimuthal distribution. For hard scattering processes in QCD mediated by quarks or gluons the particle direction may be replaced by the parton (or associated jet) direction. The decomposition of the cross-section into contributions from different photon helicity amplitudes leads to a formula with 13 measurable terms, each having a different azimuthal dependence, which may be expressed as $\cos\phi_i$ where the ϕ_i $(i = 1, 13)$ are different linear functions of ϕ and ϕ_a. The coefficients of $\cos\phi_i$ depend on the helicity states of the colliding photons, and may be considered as 'structure functions' in addition to the well known transverse and longitudinal ones that contribute to the first term, given by $\phi_1 = 0$, that corresponds to the cross-section integrated over ϕ, ϕ_a. The full 13 term formula is given by Kessler in Ref.[24].

Because of the typically low efficiences ($\simeq 1\%$) for double tagging, it is experimentally much easier to measure ϕ_a only and integrate over ϕ (single tagging experiment). In this case the full statistics of single-tagged events contributes to the azimuthal distribution.

One case where a complete measurement of the azimuthal correlations may be possible [26] is at the KLOE detector at DAΦNE, which will be equipped with a $\simeq 0°$ tagging system of high acceptance. Some predicted azimuthal distributions for the process $e^+e^- \to \pi^+\pi^-e^+e^-$ with $W_{\gamma\gamma} \leq 450$ MeV are shown in Fig. 6. The model used is based an chiral symmmety. Markedly different predictions (especially for ϕ_1 and ϕ_2) are given by a simple pion Born term.

If only single tag events are used, as in the case of the analysis of the process $e^+e^- \to \mu^+\mu^-e^+e^-$ presented here by the L3 collaoration [25], only three independant terms remain, and so the differential cross section may be written as:

$$\frac{d^3\sigma}{dxdyd\Omega} = \frac{2\pi\alpha^2}{Q^2}\frac{[1+(1-y)^2]}{xy}[A_1 + A_2\cos\phi_a + A_3\cos 2\phi_a] \tag{5}$$

$$d\Omega = d(\cos\theta)d\phi_a, \quad x = Q^2/2(k\cdot q), \quad y = (k\cdot q)/(k\cdot p), \quad Q^2 = -q^2$$

k,q,p are the 4-vectors of the target photon, probe photon and the incoming electron associated with the probe photon respectively. The angle θ is that between the μ^+ direction and the $\gamma\gamma$ axis. The coefficients A_1,A_2,A_3 can be expressed in terms of three 'structure functions' $\tilde{F}_2$, $\tilde{F}_A$, $\tilde{F}_B$, according to the relations:[d]

$$A_1 \simeq \tilde{F}_2 = 2x\tilde{F}_T + \tilde{F}_L \tag{6}$$

$$A_2 \simeq -\tilde{F}_A \tag{7}$$

$$A_3 \simeq \frac{1}{2}\tilde{F}_B \tag{8}$$

For the case $\gamma\gamma \to \mu^+\mu^-$, $\tilde{F}_T$, $\tilde{F}_L$,$\tilde{F}_A$, $\tilde{F}_B$, are precisely known [14,27e] pure QED quantities :

$$\tilde{F}_T = \frac{\alpha}{2\pi}[x^2 + (1-x)^2]\frac{1+(\beta z)^2}{1-(\beta z)^2} \tag{9}$$

$$\tilde{F}_L = \tilde{F}_B = \frac{4\alpha}{\pi}x^2(1-x) \tag{10}$$

$$\tilde{F}_A = \frac{4\alpha}{\pi}x(1-2x)\sqrt{x(1-x)}\frac{z}{\sqrt{1-(\beta z)^2}} \tag{11}$$

[d]The tilde over the 'structure function' indicates that it is a function of both x and z ($= \cos\theta$). The usual structure functions F_2,F_L are recovered by integrating $\tilde{F}_2$, $\tilde{F}_L$ over z. The $\simeq$ symbol used in Eqs. (6-7) indicates that $\gamma\gamma$ luminosity functions $\propto 1-y$ have been set to one. Also it is assumed in Eqs.(6-11) that the target photon is purely transverse

[e]There are some errors in the equations given in Ref.[14]. In Eqs.(21) a factor $\frac{1}{2}$ is missing in the first equation, a factor x in the third one.

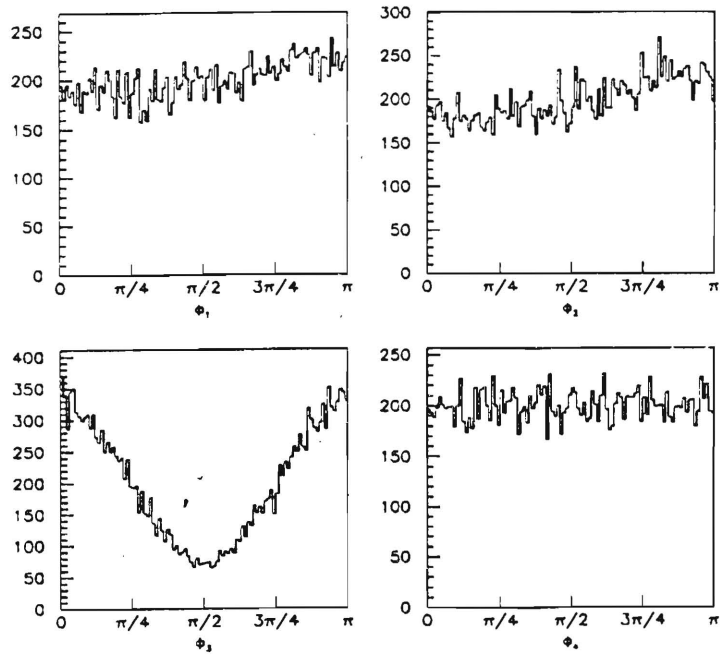

Figure 6: Predicted azimuthal angular distributions (from a chiral symmetry model) for the process $e^+e^- \rightarrow \pi^+\pi^-e^+e^-$ at KLOE. $\phi_1 = \phi_a$, $\phi_2 = \phi - \phi_a$, $\phi_3 = \phi$, $\phi_4 = 2\phi_a - \phi$ (Ref.[26]).

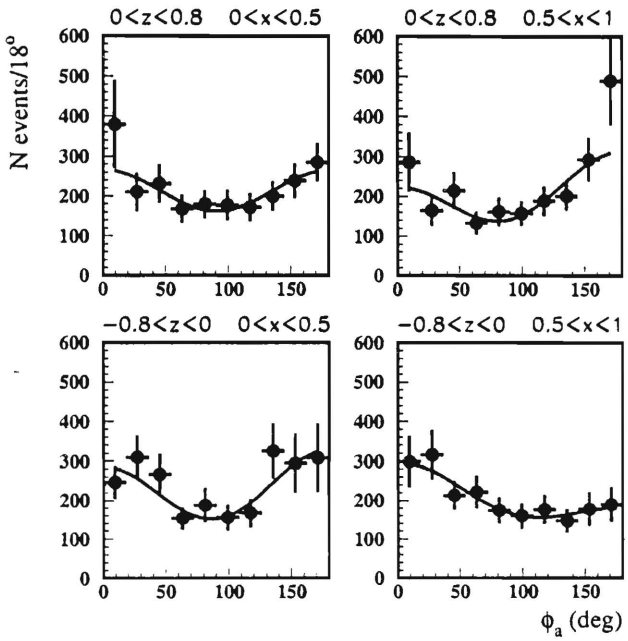

Figure 7: Distributions of ϕ_a for the process $e^+e^- \rightarrow \mu^+\mu^-e^+e^-$ as measured by the L3 Collab. (Ref.[25]).

In Eqs. (9-11) $z = \cos\theta$, $\beta = \sqrt{1 - 4xm_\mu^2/[Q^2(1-x)]}$.

The acceptance corrected ϕ_a distributions from the L3 analysis are presented in Fig.7 and a comparison with theoretical predictions in Table1. Satisfactory agreement is found within the rather large (dominantly statistical) errors. The measured distributions were fitted to functions of the form:

$$\frac{dN}{d\phi_a} = C[1 + A\cos\phi_a + B\cos 2\phi_a] \tag{12}$$

The predictions for A,B given in Table1 were obtained by integrating Eqs.(5-11) over the relevant ranges of x and z.

For a single tag experiment experiment where an anti-tag condition is imposed for the target photon (as was done in the L3 experiment) the target photon is almost real and so, to a very good approximation, purely transverse. There are then only three possible independent helicity amplitudes, specified by the value of the total photon helicity λ:

$$A(\lambda = 1), \qquad \lambda_p = 0, \qquad \lambda_t = \pm 1$$

$$A(\lambda = 0), \qquad \lambda_p = \pm 1, \qquad \lambda_t = \pm 1$$

$$A(\lambda = 2), \qquad \lambda_p = \pm 1, \qquad \lambda_t = \mp 1$$

Here λ_p,(λ_t)are the helicity projections of the probe (target) photon. The 'structure functions' defined above depend in the following way on these helicity amplitudes:

$$\tilde{F}_T \propto |A(\lambda = 0)|^2 + |A(\lambda = 2)|^2 \tag{13}$$
$$\tilde{F}_L \propto |A(\lambda = 1)|^2 \tag{14}$$
$$\tilde{F}_A \propto 2\Re e\{A(\lambda = 1)^*[A(\lambda = 0) + A(\lambda = 1)]\} \tag{15}$$
$$\tilde{F}_B \propto 2\Re e\{A(\lambda = 0)^* A(\lambda = 2)\} \tag{16}$$

Two remarks are in order. (i) Although $\tilde{F}_L$ and $\tilde{F}_B$ are the same function of x and z (and, in the literature both typically referred to as 'F_L') their helicity structures are quite different. Indeed, $\tilde{F}_B$ is purely transverse. (ii) $\tilde{F}_A$ is sensitive to the amplitude $A(\lambda = 1)$ whose square (Eq.(14)) is the well known longitudinal structure function. The latter is difficult to measure because it appears in the cross section formula multiplied by the small factor y^2. The azimuthal coefficient A_2 gives access to the same amplitude with improved experimental sensitivity.

An interesting remark was made by H.Paar during the workshop [28]. In principle it is not always necessary to observe one of the scattered electrons in order to measure the angle ϕ_a. In untagged events the plane of the tagged electron may be replaced, approximately, by the direction of the missing transverse momentum vector of the

Ranges		Experiment		Theory	
Δx	Δz	A	B	A	B
0 - 0.5	0 - 0.8	0.00 ± 0.10	0.24 ± 0.09	0.18	0.18
0.5 - 1	0 - 0.8	-0.22 ± 0.11	0.31 ± 0.09	-0.18	0.18
0 - 0.5	-0.8 - 0	-0.09 ± 0.11	0.34 ± 0.09	-0.18	0.18
0.5 - 1	-0.8 - 0	0.28 ± 0.10	0.18 ± 0.09	0.18	0.18

Table 1: Azimuthal correlations: fit results and theory comparison for the chosen x and z ranges

$\gamma\gamma$ final state. All final state particles must be observed if the p_T imbalance is to be assigned uniquely to an unseen scattered electron, so the method is limited to final states of low multiplicity.[f] Similarly ϕ may be measured by replacing the plane of the second scattered electron by the direction of the missing transverse momentum in single tagged events.

It is clearly interesting to study QCD structure function effects by using jet directions to define the angle ϕ_a [29]. So far no experiments have been performed in $\gamma\gamma$ interactions. The first results of a similar analysis in low Q^2 electroproduction by the H1 collaboration at HERA have, however been recently presented [30].

4. Transition Form Factors of the Light Pseudoscalar Mesons

Impressive new experimental results on the transition form factors of the π^0, η and η' in the range $2 < Q^2 < 16GeV^2$ from the CLEO II collaboration were presented here by V.Savinov [31]. They were matched on the theoretical side, by new HSA (Hard Scattering Approach) calculations described by P.Kroll[32].

The Born term of the transition form factor $F_{P\gamma}(Q^2)$, ($P = \pi^0,\ \eta,\ \eta'$) is a pure QED process (Fig.8). The new calculations have included for the first time the leading QCD corrections due to gluon exchange (real and virtual) summed to all orders, as well as the effect of the non zero transverse momentum of the constituent quarks. The result, for the π^0, is:

$$F_{\pi\gamma}(Q^2) = \int dx_1 \frac{d^2b}{4\pi} \tilde{\Psi}_0(x_1, -\vec{b}) \tilde{T}_H(x_1, \vec{b}, Q) \exp[-S(x_1, b, Q)] \tag{17}$$

where:

$\tilde{\Psi}_0(x_1, -\vec{b})$ = pion wave function

$\tilde{T}_H(x_1, \vec{b}, Q)$ = perturbative hard scattering amplitude

$\exp[-S(x_1, b, Q)]$ = Sudakov factor

[f] It is possible that the missing p_T receives contributions from both scattered electrons. However for values of $|p_t|$ of the order of $W_{\gamma\gamma}$ required, according to Eqs.(6-11), to give not too small values of A_1 and A_2, the effect of a single scattered electron should dominate

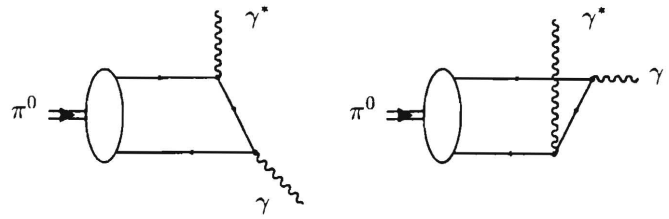

Figure 8: Lowest order graphs for the π^0 transition form factor.

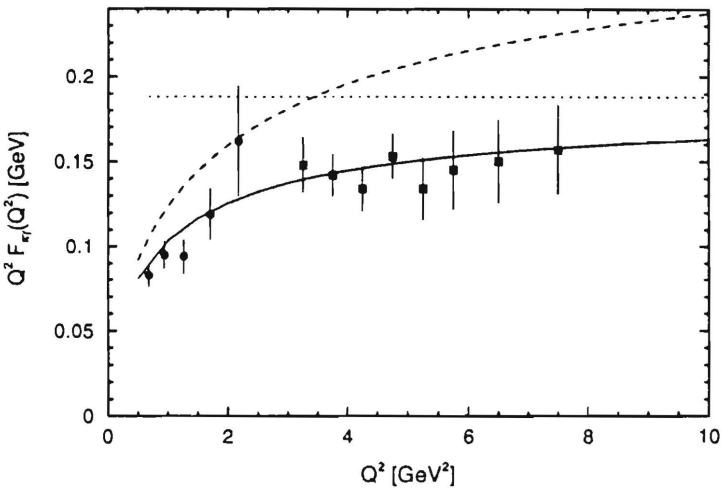

Figure 9: $Q^2 F_{\pi\gamma}(Q^2)$ versus Q^2. Solid circles CELLO data, solid squares CLEO II data (Ref[31]). Solid curve ϕ_{AS}, dashed curve ϕ_{CZ}, dotted line asymptotic result (Ref[32]).

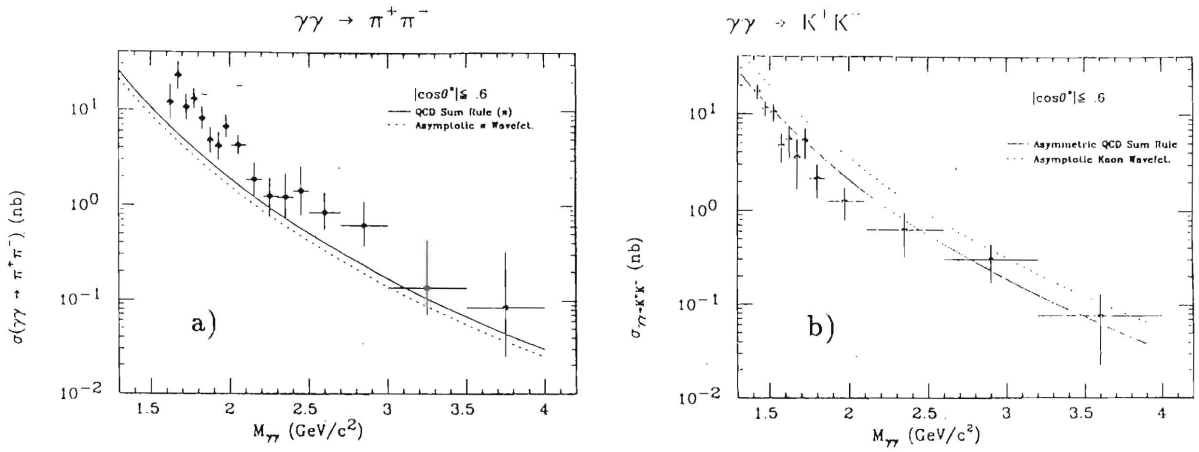

Figure 10: a) $\sigma_{\gamma\gamma} \to \pi^+\pi^-$, b) $\sigma_{\gamma\gamma} \to K^+K^-$. TPC-2$\gamma$ Collab. (preliminary). Solid lines ϕ_{CZ}, dashed lines ϕ_{AS} (Ref.[34]).

x_1, $1 - x_1$ are the fractions of the light cone momentum of the π carried by its constituent quarks and $\vec{b}$ is their spatial separation. The b dependence factors out in $\tilde{\Psi}_0$ giving:

$$\tilde{\Psi}_0(x_1, \vec{b}) = \frac{2\pi}{\sqrt{6}}\phi(x_1)\exp[-x_1 x_2 b^2/4a^2] \tag{18}$$

The free parameter a is fixed by the measured value of $\Gamma_{\gamma\gamma}(\pi^0)$. Two alternative forms of the reduced wavefunction $\phi(x_1)$ have been used to compare with the experimental results:

$$\phi_{AS} = 6x_1(1 - x_1) \tag{19}$$

$$\phi_{CZ} = 30x_1(1 - x_1)(2x_1 - 1) \tag{20}$$

ϕ_{AS} (the asymptotic form of all wavefunctions give by QCD evolution as $Q \to \infty$) is peaked around $x_1 = 0.5$, whereas the Chernyak Zhitnisky [33] wavefunction ϕ_{CZ} vanishes for $x_1 = \frac{1}{2}$ and peaks symmetrically for large and small values of x_1.

The comparison between theory and experiment for the quantity $Q^2 F_{\pi\gamma}(Q^2)$ is shown in Fig.9. ϕ_{AS} gives excellent agreement with the data. whereas ϕ_{CZ} is completely excluded, especially by the new CLEO II data with $Q^2 > 3GeV^2$. Two cautionary remarks may be made: firstly, the experimental data are equally well fitted by a VDM type form factor of the type; $(1 + Q^2/M^2)^{-2}$ where $M \simeq m_\rho$ [31]. Secondly,G.Greenbaum (TPC-2γ collaboration) [34] showed new results on $\gamma\gamma \to \pi^+\pi^-, K^+K^-$ cross sections. Although the agreement with the lowest order HSA predictions [35] is poor (especially for $\gamma\gamma \to \pi^+\pi^-$) the data does show some preference for the CZ wavefunction (Fig.10). Kroll and collaborators are now working on a new HSA calculation for these processes, incorporating the same improvements as made in the recent $F_{P\gamma}$ calculations [36]. Since the Born term for meson production is a QCD process larger theoretical uncertainties are however to be expected.

Kroll also presented a combined analysis of transition form factors and two photon decay widths in terms of the η, η' SU(3) mixing parameters [32]. The following results were found for the singlet and octet parameters f_1, f_8 and the octet/singlet mixing angle θ_P :

$$f_1 = 145 \pm 3MeV, \quad f_8 = 136 \pm 10MeV, \quad \theta_P = -18^\circ \pm 2^\circ$$

The value of f_8 seems somewhat smaller than the chiral perturbation theory prediction of Gasser and Leutwyler [37] of $170 \pm 7MeV$.

5. The Production of the Final State $\Lambda\bar{\Lambda}X$ in $\gamma\gamma$ Interactions

Preliminary CLEO II results on the process $\gamma\gamma \to \Lambda\bar{\Lambda}X$ based on $2.9fb^{-1}$ of data were presented by H.Paar[38]. Selecting events with 4 charged charge tracks, net

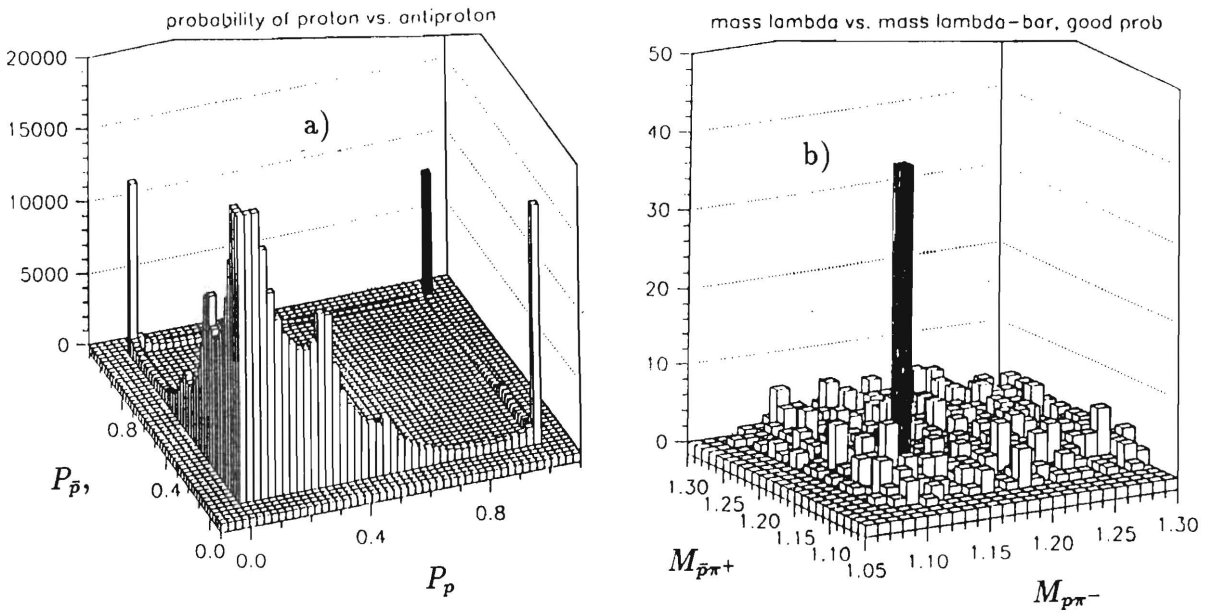

Figure 11: a) $p\bar{p}$ signal, b) $\Lambda\bar{\Lambda}$ signal (see text) CLEO II Collab. (preliminary) (Ref.[38]).

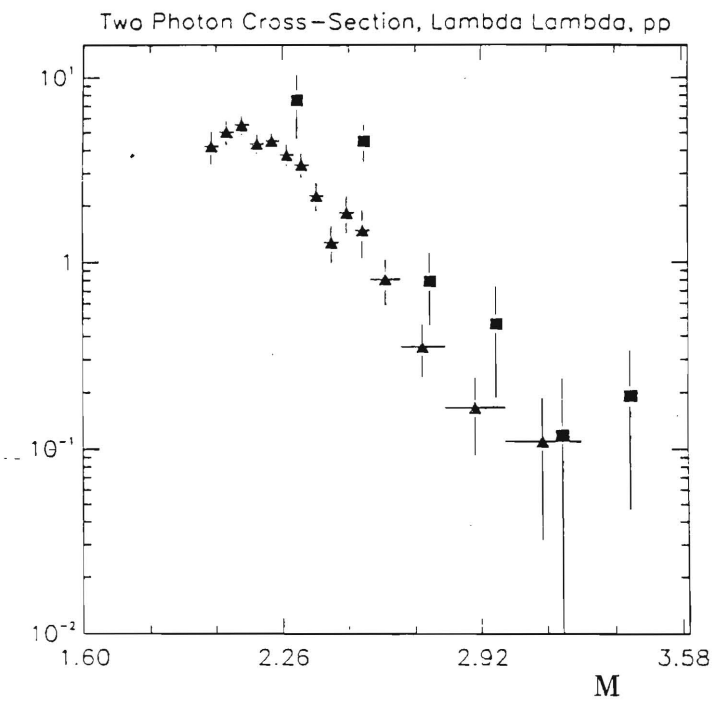

Figure 12: $p\bar{p}$ (solid triangles), $\Lambda\bar{\Lambda}$ (solid squares) cross sections as a function of M(baryon antibaryon). CLEO II (preliminary) (Ref.[38]).

charge zero, visible energy $< 6GeV$ (to remove 1γ annihilation events) and a loose vertex cut, leads to the clear signal for identified $p\bar{p}$ pairs shown in Fig.11a). The probabilities P_p, $P_{\bar{p}}$ for a track to be a p,$\bar{p}$ are given by combining dE/dX and time of flight information. A signal of 37 $\Lambda\bar{\Lambda}$ events over a low background is seen on a plot of $M(p\pi^-)$ v $M(\bar{p}\pi^+)$ (Fig.11b)). The acceptance corrected M ($\Lambda\bar{\Lambda}$ effective mass) distribution is shown in Fig.12 in comparison to the previously measured $p\bar{p}$ cross section [39]. Very surprisingly the $\Lambda\bar{\Lambda}X$ cross section is found to be considerably larger than the exclusive $p\bar{p}$ cross section!

Some theoretical predictions, based on a diquark model [40], (in very good agreement with the measured exclusive $p\bar{p}$ cross section [39]) for various exclusive baryon anti-baryon channels are shown in Fig.13. The cross sections for the $\Lambda\bar{\Lambda}$, $\Sigma^0\overline{\Sigma^0}$ channels are predicted to lie well below that for $p\bar{p}$. The summed p_T distribution of the observed $\Lambda\bar{\Lambda}$ pairs is much wider than that of an exclusive $\Lambda\bar{\Lambda}$ Monte Carlo, indicating the importance of inclusive backgrounds $\Lambda\bar{\Lambda}X$ where the particle (or particles) X remain undetected. More work is needed (Monte Carlo studies of final states contributing to $\Lambda\bar{\Lambda}X$, more stringent experimental cuts to isolate exclusive $\Lambda\bar{\Lambda}$ production) before a clear contradiction with the predictions of Ref.[40] can be demonstrated. Since photons couple to quark charges it is indeed surprising that the cross section for $\Lambda\bar{\Lambda}$ (the Λ contains two quarks of charge $-\frac{1}{3}$, one of charge $\frac{2}{3}$) should be greater than that for $p\bar{p}$ where the p contains two quarks of charge $\frac{2}{3}$, and one of charge $-\frac{1}{3}$.

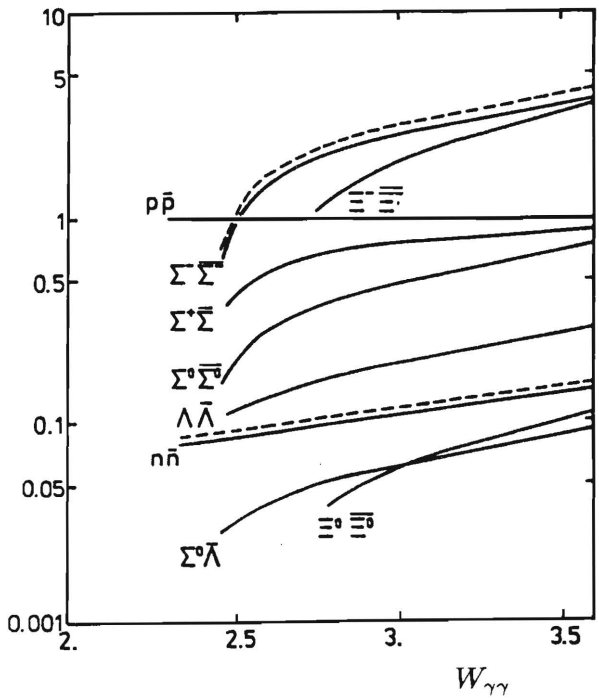

Figure 13: Predictions for $\gamma\gamma \rightarrow$hyperon+antihyperon cross sections as a function of $W_{\gamma\gamma}$ using ϕ_{AS} (solid line) or ϕ_{CZ} (dashed line). The curves are normalised relative to $\sigma(\gamma\gamma \rightarrow p\bar{p})$ (Ref.[40])

6. Acknowledgments

On behalf of all the participants I should like to thank all members of the U.K. Organising Commitee, especially Susan Cartwright, Fred Combley, Valery Khoze and David Miller for such a remarkably successful and stimulating workshop.

7. References

1. J.H. Field, E. Pietarinen, and K. Kajantie, *Nucl. Phys.* **B171** (1980) 377
2. B. Behrens, ZEUS Collab. *These Proceedings*
3. J. Butterworth, ZEUS Collab. *These Proceedings*
4. H. Erdman, H1 Collab. *These Proceedings*
5. H. Hayashi, TOPAZ Collab. *These Proceedings*
6. M. Iwasaki, TOPAZ Collab. *These Proceedings*
7. G. Marchesini *et al.*, *Comp. Phys. Comm.* **67** (1992) 465 CPHCB
8. H. Abramowicz, K. Charchula and A. Levy, *Phys. Lett.* **269B** (1991) 458
9. M. Gluck, E. Reya and A. Vogt, *Z. Phys.* **C53** (1992) 651
10. S. Catani,Yu L. Dokshitzer, M.H.Seymour and B.R. Webber, *Nucl. Phys.* **B406** (1993) 187
11. S. Catani,Yu L. Dokshitzer and B.R. Webber, *Phys. Lett.* **285B** (1992) 291
12. H.U. Bengtsson and T. Sjöstrand, *Comp. Phys. Comm.* **46** (1987) 43,T. Sjöstrand, CERN-TH 6488/92
13. P. Aurenche, *These Proceedings*
14. C. Peterson, T.F. Walsh, P.M. Zerwas, *Nucl. Phys.* **B229** (1983) 301
15. J.H. Field, F. Kapusta and L. Poggioli, *Phys. Lett.* **181B** (1986) 362 and *Z. Phys.* **C36** (1987) 121 F. Kapusta,*Z. Phys.* **C42** (1989) 225
16. J.H. Field *Il Nuovo Cimento*, Vol. 104A N.1 (1991) 25
17. M. Althoff *et al.*, TASSO Collab. *Phys. Lett.* **138B** (1984) 219
18. Ch. Berger *et al.*, PLUTO Collab. *Z. Phys.* **C26** (1984) 191, **C29** (1985) 225 and **C33** (1987) 351
19. C.H. Llewellyn-Smith, *Phys. Lett.* **79B** (1978) 83
20. J.H. Field in *Proceedings of the VIII International Workshop on Photon-Photon Collisions* Shoresh, Israel, 1988. Ed. Uri Karshon. World Scientific P349
21. G.A. Schuler and T. Sjöstrand *Phys. Lett.* **300B** (1993) 169 and *Nucl. Phys.* **B407** (1993) 539
22. F. Kapusta, *These Proceedings*
23. G.A. Schuler,*These Proceedings* G.A. Schuler and T. Sjöstrand CERN-TH/95-62, LU TP 95-6

24. P. Kessler, *These Proceedings*
25. E. Leonardi, *These Proceedings*
26. A. Courau, private communication and Frascati pre-print LNF-93/030 (P)
27. CELLO Collab., H.J. Behrend *et al.*, *Z. Phys.* **C43** (1989) 1
28. H. Paar, private communication
29. A. Higuchi *et al.*, *Phys. Rev.* **24D** (1981) 1191
30. A. De Roeck DESY 95-025 March 1995 C. Jacobsson, PhD thesis Univ. Lund 1994
31. V. Savinov, *These Proceedings*
32. P. Kroll, *These Proceedings* and Univ. Wuppertal pre-print WU-394-28 October 1994
33. V.L. Chernyak and A.R. Zhitnitsky, *Nucl. Phys.* **B201** (1982) 492
34. G. Greenbaum, *These Proceedings*
35. S.J. Brodsky and G.P. Lepage, *Phys. Rev.* **24D** (1981) 1808
36. P. Kroll, private communication
37. G.Gasser and H. Leutwyler, *Nucl. Phys.* **B250** (1985) 465
38. H. Paar, *These Proceedings*
39. M. Artuso *et al.*, 1993. CLNS pre-print 93/1245
40. M. Anselmino *et al.*, *Int J. Mod. Phys.* **A4** (1989) 5213

IMPAE

NAME	I D No.	M.S.

RCTI LAB LIBRARY